SF2A 2017
C. Reylé, P. Di Matteo, F. Herpin, É. Lagadec, A. Lançon, Z. Meliani, F. Royer (eds)

THE WEAK LENSING ANALYSIS OF THE CFHTLS AND NGVS REDGOLD GALAXY CLUSTERS

C. Parroni[1], S. Mei[1,2], T. Erben[3], L. Van Waerbeke[4], A. Raichoor[5], J. Ford[6], R. Licitra[1,], M. Meneghetti[7], H. Hildebrandt[3,], L. Miller[8], P. Côté[9], G. Covone[10], J.-C. Cuillandre[11], P.-A. Duc[12], L. Ferrarese[9,], S. D. J. Gwyn[9,] and T. H. Puzia[13]

Abstract. An accurate estimation of galaxy cluster masses is essential for their use in cosmological and astrophysical studies. We studied the accuracy of the optical richness obtained by our RedGOLD cluster detection algorithm (Licitra et al. 2016a,b) as a mass proxy, using weak lensing and X-ray mass measurements. We measured stacked weak lensing cluster masses for a sample of 1323 galaxy clusters in the Canada-France-Hawaii Telescope Legacy Survey W1 and the Next Generation Virgo Cluster Survey at $0.2 < z < 0.5$, in the optical richness range 10-70. We tested different weak lensing mass models that account for miscentering, non-weak shear, the two-halo term, the contribution of the Brightest Cluster Galaxy, and the intrinsic scatter in the mass-richness relation. We calculated the coefficients of the mass-richness relation, and of the scaling relations between the lensing mass and X-ray mass proxies.

Keywords: weak lensing, galaxy clusters, scaling relations

1 Introduction

Galaxy clusters are the largest and most massive gravitationally bound systems in the universe and have proven to be fundamental tools to probe the current ΛCDM model and structure formation scenarios. The study of their properties, such as their correlation function and power spectrum, their baryonic fraction, the halo mass function and its evolution, requires accurate mass measurements and a full understanding of the systematics and biases involved in the analysis to better calibrate the scaling relations between cluster mass and observables that correlate with it. Because cluster masses cannot be measured directly, we need to rely on mass proxies. The

[1] LERMA, Observatoire de Paris, PSL Research University, CNRS, Sorbonne Universités, UPMC Univ. Paris 06, F-75014 Paris, France, University of Paris Denis Diderot, University of Paris Sorbonne Cité (PSC), F-75205 Paris Cedex 13, France

[2] Jet Propulsion Laboratory, Cahill Center for Astronomy & Astrophysics, California Institute of Technology, 4800 Oak Grove Drive, Pasadena, California, USA

[3] Argelander-Institut für Astronomie, University of Bonn, Auf dem Hügel 71, D-53121 Bonn, Germany

[4] Department of Physics and Astronomy, University of British Columbia, 6224 Agricultural Road, Vancouver, B.C., V6T 1Z1, Canada

[5] Institute of Physics, Laboratory of Astrophysics, Ecole Polytechnique Fédérale de Lausanne (EPFL), Observatoire de Sauverny, 1290 Versoix, Switzerland

[6] *e*Science Institute, University of Washington, Campus Box 351570, Seattle, WA 98195, USA

[7] INAF - Osservatorio Astronomico di Bologna, Bologna, Italy & INFN, Sezione di Bologna, Bologna, Italy

[8] Department of Physics, University of Oxford, Denys Wilkinson Building, Keble Road, Oxford OX1 3RH, U.K

[9] National Research Council of Canada, Herzberg Astronomy and Astrophysics Program, 5071 West Saanich Road, Victoria, BC, V9E 2E7, Canada

[10] INAF Osservatorio Astronomico di Capodimonte, Dipartimento di Fisica, University of Naples Federico II, INFN, Via Cinthia, I-80126 Napoli, Italy

[11] CEA/IRFU/SAp, Laboratoire AIM Paris-Saclay, CNRS/INSU, Université Paris Diderot, Observatoire de Paris, PSL Research University, F-91191 Gif-sur-Yvette Cedex, France

[12] AIM Paris-Saclay Service d'astrophysique, CEA-Saclay, F-91191 Gif sur Yvette, France, Université de Strasbourg, CNRS, Observatoire astronomique de Strasbourg, UMR 7550, F-67000 Strasbourg, France

[13] Institute of Astrophysics, Pontificia Universidad Católica de Chile, Av. Vicuña Mackenna 4860, 7820436 Macul, Santiago, Chile

aim of our work was to infer galaxy cluster masses using weak lensing measurements, through the reconstruction of their stacked shear profiles, and to calibrate the precision of the RedGOLD optical richness (Licitra et al. 2016a,b) as a mass proxy.

For our analysis, we used our own data reduction (Raichoor et al. 2014) of the Canada-France-Hawaii Telescope Legacy Survey (CFHT-LS; Gwyn 2012) Wide 1 (W1) field and of the Next Generation Virgo Cluster Survey (NGVS; Ferrarese et al. 2012). Galaxy clusters were detected using the RedGOLD optical cluster finder of Licitra et al. (2016a,b). The shear measurements come from the CFHTLenS W1 (Heymans et al. 2012; Erben et al. 2013) and NGVSLenS (Raichoor et al. 2014) catalogs and were obtained using the *lens*fit algorithm (Miller et al. 2013). Photometric redshifts were determined by Raichoor et al. (2014), using the bayesian codes BPZ (Benítez 2000) and *LePhare* (Arnouts at al. 1999). In order to have the most clean and complete sample, we restricted the analysis to clusters with redshift $0.2 < z < 0.5$ and richness $10 < \lambda < 70$, bringing the final catalog to a total of 1323 clusters. For the calculation of the scaling relations between lensing masses and X-ray mass proxies, we used Gozaliasl et al. (2014) X-ray catalog, based on the *XMM-Newton* observations in the ~ 3 deg^2 overlapping the CFHT-LS W1 field.

2 Weak lensing analysis

We calculated the mean shear radial profiles, stacking clusters binned according to their optical richness and averaged the tangential shear in logarithmic radial bins, applying lens-source pairs weights that depend on the lensing efficiency and on the quality of background galaxy shape measurements. We calculated the errors on each profile point using the bootstrap technique, taking clusters with replacements within each richness bin.

We fitted these profiles assuming a *Basic Model* that consists in a halo model (Seljak 2000), with an NFW (Navarro, Frenk & White 1996) surface density contrast, and correction terms that take into account cluster miscentering (Johnston et al. 2007; George et al. 2012), non-weak shear (Mandelbaum et al. 2006; Johnston et al. 2007) and the two halo term (Seljak 2000; Seljak & Warren 2004; Johnston et al. 2007). We then considered extensions of this model including the intrinsic scatter in the mass-richness relation, in the *Added Scatter Model*, and the contribution of the Brightest Cluster Galaxy (BCG), in the *Two Component Model*. In all cases, we used the concentration-mass relation of Dutton & Macció (2014), to reduce the dimensionality of the problem. The study of these models allowed us to constrain the contribution of each corrective term and to better understand the biases and systematics involved in the analysis.

In order to estimate the error bars on the fitting parameters, we run Markov Chains Monte Carlo (MCMC; Metropolis et al. 1953) with the Python package *emcee* (Foreman-Mackey et al. 2013), which allowed us to efficiently sample the model likelihood. In Fig. 1, on the left, we find the shear profiles, with the data (in black), the fit results (in green), the ideal profiles we would get in case all the clusters in the stack were perfectly centered (in red), and the opposite case (in blue). On the right, we can see the lensing signal-to-noise ratio map for the corresponding stack of clusters, obtained using aperture mass statistics (Schneider 1996; Schirmer et al. 2006; Du & Fan 2014).

3 Results

3.1 Mass–richness relation

We performed a fit to a power law to infer the mass–richness relation for all three models, using the lensing masses calculated for each richness bin: $\log M_{200} = \log M_0 + \alpha \log \lambda/\lambda_0$, with a pivot richness $\lambda_0 = 40$. We show the results in Fig. 2, on the left.

Because the *Basic* and the *Two Component Models* do not include the intrinsic scatter in the mass–richness relation as a free parameter in the fit, we applied an a posteriori correction as in Ford et al. (2015) to take this effect into account. Starting from the mass–richness relation inferred from the *Basic Model* and from the *Two Component Model*, we assigned a mass to each cluster in the sample, then we scattered them assuming a log-normal distribution centered on $\log M_{200}$ and with a width $\sigma_{\ln \mathrm{M}|\lambda} = 0.39$, based on the scatter measured by Licitra et al. (2016a). We then fitted the mass-richness relation using the new mean mass values in each richness bin, obtaining a difference in normalization between the original models and their scattered versions that is less than 1%. In Table 1, we summarize the slope and the normalization values obtained with the different models. All results are consistent within 1σ.

Having verified the impact of each model term on the final results, we consider as our *Final Model* the model that takes into account all the parameters considered so far, the *Two Component Model* with the a posteriori

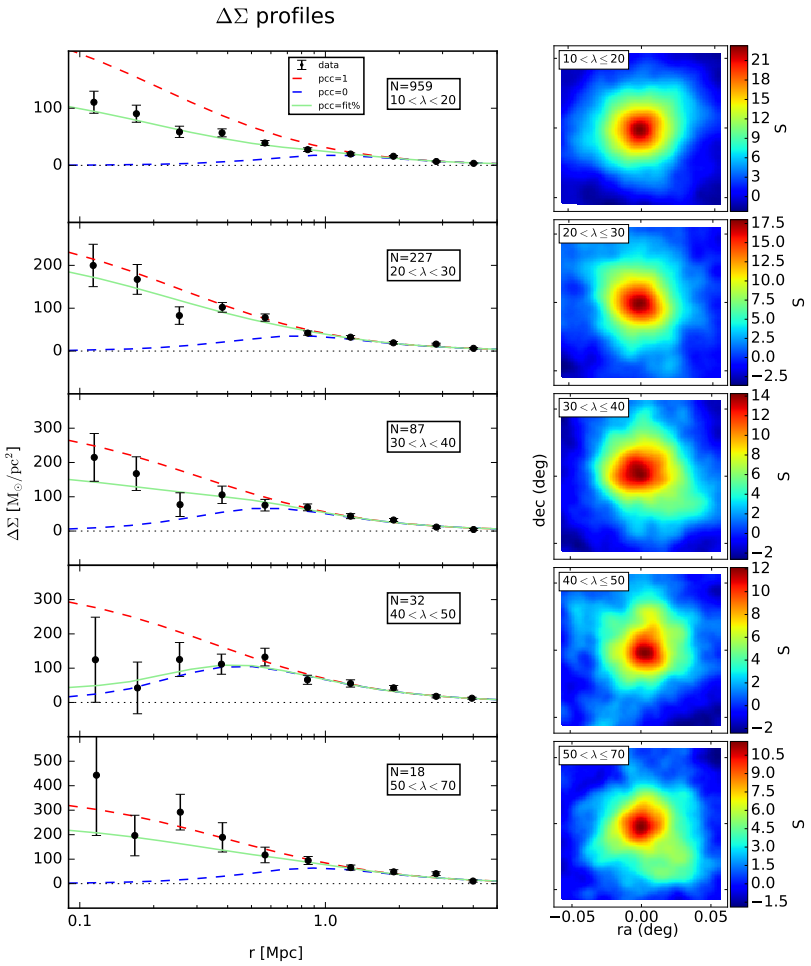

Figure 1. Left: Shear profile measurement (black), the fit results (green), the ideal profiles that we would obtain in the case in which all the clusters in the stack were perfectly centered (red) and when they would have been all miscentered (blue). The fits were obtained using the *Basic Model*, and we get similar results using the *Added Scatter* and the *Two Component Models*. **Right:** Lensing signal-to-noise ratio maps in each richness bin for our weak lensing selected sample. We applied aperture mass statistics.

intrinsic scatter correction. Our final mass–richness relation is then: $\log M_0 = 14.46 \pm 0.02$ and $\alpha = 1.04 \pm 0.09$.

Table 1. Results of the fit of the mass–richness relation obtained using the three models. For the Basic and Two Component Models, we also show the results after applying the a posteriori intrinsic scatter correction (ISC).

Model	$\log M_0$	α
Basic	14.43 ± 0.01	1.05 ± 0.07
Basic + ISC	14.47 ± 0.02	1.05 ± 0.09
Added Scatter	14.42 ± 0.03	0.97 ± 0.14
Two Component	14.43 ± 0.01	1.05 ± 0.07
Two Component + ISC	14.46 ± 0.02	1.04 ± 0.09

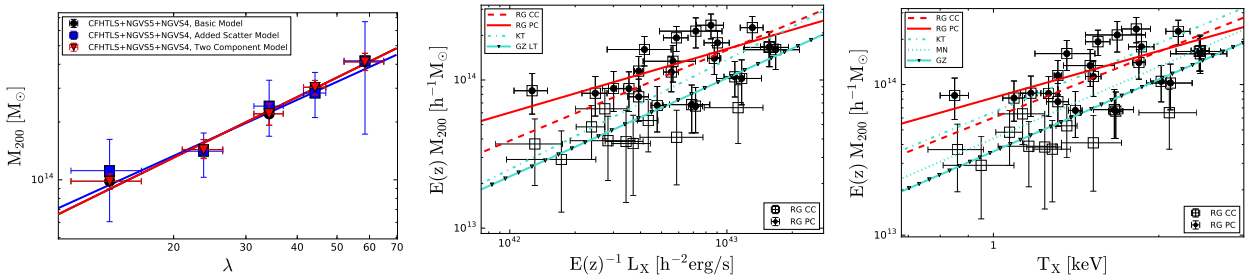

Figure 2. Left: The weak lensing mass–richness relations obtained using the *Basic Model* (black line and black dots), *Added Scatter Model* (blue line and blue squares), and *Two Component Model* (red line and red triangles). **Center:** The weak lensing mass vs X-ray luminosity relation, in red, derived matching our cluster sample with Gozaliasl et al. (2014) (GZ) X-ray catalog, compared with those of Leauthaud et al. (2010) (LT) and Kettula et al. (2015) in cyan. **Right:** The weak lensing mass vs X-ray temperature relation, in red, compared with those of Kettula et al. (2015) (KT) and Mantz et al. (2016) (MN).

As shown in Licitra et al. (2016a,b), our richness estimator λ is defined in a similar way as the richness from redMaPPer (Rykoff et al. 2014). We can then compare our results with others obtained through a similar stacking lensing analysis or different techniques (i.e. velocity dispersions, abundance matiching), using the redMaPPer cluster sample (Rykoff et al. 2012; Saro et al. 2015; Farahi et al. 2016; Melchior et al. 2016; Simet et al. 2016). Our normalization is in perfect agreement with all the works cited above ($< 1\sigma$). On the other hand, there is a slight tension between our slope and those of Simet et al. (2016) and Farahi et al. (2016) ($1.5 - 2\sigma$), but not with Rykoff et al. (2012), Saro et al. (2015), and Melchior et al. (2016) ($< 1\sigma$).

3.2 Lensing mass versus X-ray mass proxies relations

In order to compare our lensing mass estimates with X-ray mass proxies, we used Gozaliasl et al. (2014) X-ray catalog. We applied a logarithmic linear fit, in the form: $\log\left(\frac{M_{200}E(z)}{M_0}\right) = a + b\log\left(\frac{L_X}{L_0 E(z)}\right)$ and $\log\left(\frac{M_{200}E(z)}{M_0}\right) = a + b\log\left(\frac{T_X}{T_0}\right)$, where $E(z) = H(z)/H_0$, $M_0 = 8 \times 10^{13}\ h^{-1}M_\odot$ for the $M_{200} - L_X$, $M_0 = 6 \times 10^{13}\ h^{-1}M_\odot$ for the $M_{200} - T_X$, $L_0 = 5.6 \times 10^{42}\ h^{-2}erg/s$, and $T_0 = 1.5\ keV$.

For the mass–luminosity relation, we find $a = 0.10 \pm 0.03$ and $b = 0.61 \pm 0.12$, with a scatter $\sigma_{\log M_{200}|L_X} = 0.20$ dex. For the mass–temperature relation, we find $a = 0.23 \pm 0.03$ and $b = 1.46 \pm 0.28$, with a scatter $\sigma_{\log M_{200}|T_X} = 0.20$ dex. In Fig. 2, we show the mass–luminosity (center) and mass–temperature relations (right), and compare them to those of other works in literature (Leauthaud et al. 2010; Kettula et al. 2015; Mantz et al. 2016). Our results are consistent with those of the other works cited within $< 1\sigma$, in normalization and slope, except for Leauthaud et al. (2010) normalization ($< 2.5\sigma$).

4 Conclusions

We tested different profile models and different fitting techniques, obtaining results in good agreement with each other. In particular, the miscentering correction resulted to be the one that most affects the halo mass measurements ($10 - 40\%$), while including or not the BCG mass does not make a difference in the recovered parameters. The intrinsic scatter in the mass-richness relation is not constrained by the data, and we applied an a posteriori correction to take this factor into account.

We derived our mass–richness relation and compared it with others from the literature finding results in agreement within 1σ in most of the cases. The small slope discrepancy that we found, comparing our results to those of Farahi et al. (2016) and Simet et al. (2016), could be due to the different samples that were used (i.e. different survey depth, mean redshift, and richness estimation) and to the different analyses performed (i.e. fitting techniques, number of parameters).

Matching our sample with Gozaliasl et al. (2014) X-ray catalog, we derived the coefficients of the mass–luminosity and mass–temperature relations, and compared them with previous results, finding good agreement. In particular, the slope values found are in perfect agreement with the predicted deviations from the self-similar mass–luminosity and mass–temperature relations, confirming the role of hydrodynamical processes, such as

radiative cooling, feedback from star formation, AGN activity, in the standard structure formation scenario (Böhringer et al. 2011).

In order to increase the accuracy of this kind of weak lensing mass estimates, it will be important to increase the number density of background sources to achieve a higher S/N in the shear profile measurements, either using deeper observation or increasing the cluster sample size. In the future, this will be possible with ground- and space-based large-scale surveys such as the LSST*, *Euclid*† and WFIRST‡ that will detect around 100,000 galaxy clusters, allowing us to constrain their masses with even higher accuracy.

This work is based on observations obtained with MegaPrime/MegaCam, a joint project of CFHT and CEA/IRFU, at the Canada-France-Hawaii Telescope (CFHT) which is operated by the National Research Council (NRC) of Canada, the Institut National des Sciences de l'Univers of the Centre National de la Recherche Scientifique (CNRS) of France, and the University of Hawaii. This research used the facilities of the Canadian Astronomy Data Centre, operated by the National Research Council of Canada with the support of the Canadian Space Agency. CFHTLenS data processing was made possible thanks to significant computing support from the NSERC Research Tools and Instruments grant program. R.L., S.M., and A.Ra. acknowledge the support of the French Agence Nationale de la Recherche (ANR) under the reference ANR10-BLANC-0506-01-Projet VIRAGE (PI: S.Mei). S.M. acknowledges financial support from the Institut Universitaire de France (IUF), of which she is senior member. H.H. is supported by the DFG Emmy Noether grant Hi 1495/2-1. We thank the Observatory of Paris and the University of Paris D. Diderot for hosting T.E. under their visitor programs.

Facilities: CFHT.

References

Arnouts, S., Cristiani, S., Moscardini, L., et al. 1999, MNRAS, 310, 540

Benítez N. 2000, ApJ, 536, 571

Böhringer, H., Dolag, K., Chon, G. 2011, A&A, 539, A120

Du, W. & Fan, Z. 2014, ApJ, 785, 57

Dutton, A. A. & Macció, A. V. 2014, MNRAS, 441, 3359

Erben, T., Hildebrandt, H., Miller, L., et al. 2013, MNRAS, 433, 2545

Farahi, A., Evrard, A. E., Rozo, E., Rykoff, E. S., Wechsler, R. H. 2016, MNRAS, 460, 3900

Ferrarese, L., Cote, P., Cuillandre, J.-C., et al. 2012, ApJS, 200, 4

Ford, J., van Waerbeke, L., Milkeraitis, M., et al. 2015, MNRAS 447, 1304

Foreman-Mackey, D., Hogg, D. W., Lang, D., Goodman, J. 2013, PASP, 125, 925

George, M. R., Leauthaud, A., Bundy, K., et al. 2012, ApJ, 757, 2

Gozaliasl, G., Finoguenov, A., Khosroshahi, H. G., et al. 2014, A&A 566, 140

Gwyn, S. D. J. 2012, ApJ, 143, 38

Heymans, C., van Waerbeke, L., Miller, L., et al. 2012, MNRAS, 427, 146

Hildebrandt, H., Erben, T., Kuijken, K., et al. 2012, MNRAS, 421, 2355

Johnston, D. E., Sheldon, E. S., Wechsler, R. H., et al. 2007, arXiv:0709.1159

Kettula, K., Giodini, S., van Uitert, E., et al. 2015, MNRAS, 451, 1460

Leauthaud, A., Finoguenov, A., Kneib, J.-P., et al. 2010, ApJ, 709, 114

Licitra, R., Mei, S., Raichoor, A., et al. 2016, ApJ, 829, 44

Licitra, R., Mei, S., Raichoor, A., Hildebrandt, H. 2016, MNRAS, 455, 3020

Mandelbaum, R., Seljak, U., Cool, R. J., et al. 2006, MNRAS, 372, 758

Mantz, A. B., Allen, S. W., Morris, R. G., et al. 2016, MNRAS, 463, 3582

Melchior, P., Gruen, D., McClintok, T., et al. 2016, arXiv:1610.06890v1

Metropolis, N., Rosenbluth, A. W., Rosenbluth, M. N., et al. 1953, JChPh, 21,1087

Miller L., Heymans, C., Kitching, T. D., et al. 2013, MNRAS, 429, 2858

Navarro J. F., Frenk C. S., White S. D. M. 1996, ApJ, 462, 563

Raichoor, A., Mei, S., Erben, T., et al. 2014, ApJ, 797, 102

Rykoff, E. S., Koester, B. P., Rozo, E., et al. 2012, ApJ, 746, 178

Rykoff, E. S., Rozo, E., Busha, M. T., et al. 2014, ApJ, 785, 104

*https://www.lsst.org/

†http://euclid- ec.org

‡http://wfirst.gsfc.nasa.gov

Saro, A., Bocquet, S., Rozo, E., et al. 2015, MNRAS, 454, 2305
Schirmer, M., Erben, T., Hetterscheidt, M., Schneider, P. 2006, A&A, 462, 875
Schneider, P. 1996, MNRAS, 283, 837
Seljak, U. 2000, MNRAS. 318, 203
Seljak, U. & Warren, M. S. 2004, MNRAS, 355, 129
Simet, M., McClintock, T., Mandelbaum, R., et al. 2016, arXiv:1603.06953v1